Neurobiology of Aging 75 (2019) 209–222

Contents lists available at ScienceDirect

Neurobiology of Aging

journal homepage: www.elsevier.com/locate/neuaging

Investigation of mitochondrial calcium uniporter role in embryonic and adult motor neurons from G93A^{hSOD1} mice

Vedrana Tadić [a,*], Adam Adam [a], Nadine Goldhammer [a], Janin Lautenschlaeger [a,b], Moritz Oberstadt [c], Ayse Malci [a], Thanh Tu Le [a], Saikata Sengupta [a], Beatrice Stubendorff [a], Silke Keiner [a], Otto W. Witte [a], Julian Grosskreutz [a]

[a] Hans Berger Department of Neurology, Jena University Hospital, Jena, Germany
[b] Department of Chemical Engineering and Biotechnology, University of Cambridge, Cambridge, UK
[c] Department of Neurology, University of Leipzig, Leipzig, Germany

ARTICLE INFO

Article history:
Received 1 August 2017
Received in revised form 16 November 2018
Accepted 17 November 2018
Available online 23 November 2018

Keywords:
ALS
SOD1
KN-62
MCU
Kaempferol
Calcium

ABSTRACT

Amyotrophic lateral sclerosis is characterized by progressive death of motor neurons (MNs) with glutamate excitotoxicity and mitochondrial Ca^{2+} overload as critical mechanisms in disease pathophysiology. We used MNs from G93A^{hSOD1} and nontransgenic embryonic cultures and adult mice to analyze the expression of the main mitochondrial calcium uniporter (MCU). MCU was overexpressed in cultured embryonic G93A^{hSOD1} MNs compared to nontransgenic MNs but downregulated in MNs from adult G93A^{hSOD1} mice. Furthermore, cultured embryonic G93A^{hSOD1} were rescued from kainate-induced excitotoxicity by the Ca^{2+}/calmodulin-dependent protein kinase type II inhibitor; KN-62, which reduced MCU expression in G93A^{hSOD1} MNs. MCU activation via kaempferol neither altered MCU expression nor influenced MN survival. However, its acute application served as a fine tool to study spontaneous Ca^{2+} activity in cultured neurons which was significantly altered by the mutated hSOD1. Pharmacological manipulation of MCU expression might open new possibilities to fight excitotoxic damage in amyotrophic lateral sclerosis.

1. Introduction

Amyotrophic lateral sclerosis (ALS) is a multisystem and multifactorial disease (Cozzolino et al., 2015; Kiernan et al., 2011) characterized by the degeneration of upper and lower motor neurons (MNs) (Martin, 2011). 90% of the patients suffer from sporadic ALS, whereas 10% develop the hereditary or familial form of ALS caused by mutations in different genes (Ingre et al., 2015). In 20% of familial ALS cases, mutations in the *SOD1* gene encoding the Cu^{2+}, Zn^{2+}-dependent superoxide dismutase are found (Rosen et al., 1993). Transgenic mice overexpressing human G93A mutant SOD1 (G93A^{hSOD1}) develop a stereotypic syndrome suggestive of MN disease making them a compelling model organism for ALS (Gurney et al., 1994). Disease mechanisms of both sporadic and familial ALS share common pathogenic features, in particular glutamate excitotoxicity, Ca^{2+} overload, and mitochondrial dysfunction (King et al., 2016; Tadic et al., 2014). Excitotoxicity is defined as cell death resulting from the toxic actions of excitatory neurotransmitters such as glutamate (King et al., 2016; Van Den Bosch et al., 2006). Overstimulation of glutamate receptors facilitates the entry and consequently the excess of Ca^{2+} in cell compartments, leading to breakdown of endoplasmic reticulum (ER) Ca^{2+} homeostasis and mitochondrial Ca^{2+} overload (Grosskreutz et al., 2010).

Intracellular Ca^{2+} concentration is regulated partially through the ER mitochondria Ca^{2+} cycle (ERMCC) (Grosskreutz et al., 2010). Briefly, after the initial α-amino-3-hydroxy-5-methyl-4-isoxazolepropionic acid receptor (AMPAR) activation, cytosolic Ca^{2+} increases and triggers more Ca^{2+} release from the ER stores (through so-called calcium-induced calcium release) via ryanodine receptors and 1,4,5-trisphosphate receptors. Subsequently, Ca^{2+} is taken up into mitochondria. Under physiological condition, mitochondria have a huge capacity to take up and accumulate Ca^{2+} from the cytosol. Physiological transport of Ca^{2+} into mitochondria is mostly facilitated by the MCU complex that is localized in the inner mitochondrial membrane. It consists of the channel-forming subunit MCU and several regulatory subunits (Kirichok et al., 2004; Marchi and Pinton, 2014). It binds Ca^{2+} with high affinity enabling high Ca^{2+} selectivity (Kirichok et al., 2004). Ca^{2+} is also

* Corresponding author at: Hans Berger Department of Neurology, Jena University Hospital, Am Klinikum 1, 07747 Jena, Germany. Tel.: +49 3641 9 396 630; Fax: +49 3641 932 3452.
E-mail address: vedrana.tadic@med.uni-jena.de (V. Tadić).

0197-4580/$ – see front matter © 2018 Elsevier Inc. All rights reserved.
https://doi.org/10.1016/j.neurobiolaging.2018.11.019

transported through the outer mitochondrial membrane by the voltage-dependent anion channel (VDAC). However, it is still not clear if the VDAC is required to channel Ca^{2+} through the outer mitochondrial membrane or if other transport proteins are involved as well (Israelson et al., 2010; Rapizzi et al., 2002). A part of released ER Ca^{2+} can also be transferred directly from the 1,4,5-trisphosphate receptor to VDAC. Accumulated Ca^{2+} in the mitochondria is slowly ejected back into the cytosol through the mitochondrial Na^{+}/Ca^{2+} exchanger. The Ca^{2+} uptake into the ER is primarily mediated by the activity of the sarcoplasmic/endoplasmic reticulum Ca^{2+}-ATPase. Several pumps and transporters in the plasma membrane maintain Ca^{2+} clearance in MNs (Grosskreutz et al., 2010). Under extreme stress conditions, such as mitochondrial Ca^{2+} overload, mitochondrial permeability transition pore is formed and apoptotic cell death is activated due to the release of cytochrome C (Martin, 2011; Martin et al., 2009).

For the induction of glutamate excitotoxicity, the presence of extracellular Ca^{2+} is decisive (Carriedo et al., 1996; Van Den Bosch et al., 2000). Although, the major Ca^{2+} inflow occurs through L-type voltage-gated Ca^{2+} channels (VGCCs) following AMPAR activation (Joshi et al., 2011), direct activation of VGCCs does not trigger Ca^{2+} accumulation or disruption of mitochondrial membrane potential in MNs (Joshi et al., 2015; Van den Bosch et al., 2002). In contrast, the similar cytosolic Ca^{2+} increase after AMPAR stimulation causes mitochondrial Ca^{2+} overload and mitochondrial depolarization (Joshi et al., 2015). Disturbances in intracellular Ca^{2+} homeostasis are known in ALS (Tadic et al., 2014), and it was postulated that they likely result in a chronic shift of Ca^{2+} from the ER to the mitochondria (Grosskreutz et al., 2010). Such a cellular state can further trigger ER stress due to perturbations in protein folding machinery, and mitochondrial Ca^{2+} overload, both of which can induce apoptosis through Bcl-2–dependent mechanisms (Jaiswal, 2014; Prell et al., 2012). MCU overexpression increases mitochondrial Ca^{2+} levels leading to increased mitochondrial membrane depolarization and excitotoxic cell death (Qiu et al., 2013). MCU knockdown diminished NMDAR-induced rise in mitochondrial Ca^{2+} reducing mitochondrial depolarization and increasing resistance to excitotoxicity (Qiu et al., 2013).

Here, we used cultured embryonic MNs and MNs from adult $G93A^{hSOD1}$ and nontransgenic mice to analyze MCU protein level as a function of disease progression. In addition, we applied different kinds of pharmacological manipulation to study mitochondrial Ca^{2+} buffering capacity, and their influence on cytosolic Ca^{2+}, neuronal survival, and MCU expression itself. Compared to nontransgenic genotype, it seems that MCU expression is remodeled during disease progression: from overexpression in embryonic $G93A^{hSOD1}$ MNs to downregulation in adult presymptomatic and symptomatic $G93A^{hSOD1}$ animals. MCU function within the ERMCC seems to be affected by the presence of $G93A^{hSOD1}$ mutation as MCU activation by kaempferol (KMF) displayed different patterns of Ca^{2+} traces when compared to nontransgenic genotype. Furthermore, pharmacological manipulation of MCU expression using KN-62 rescued $G93A^{hSOD1}$ MNs against kainate-induced cell death, thus witnessing that modulation of MCU expression might offer new approaches in rescue strategies against excitotoxicity.

2. Material and methods

2.1. Animals

The protocols for animal experiments were in compliance with the Directives of the Protection of Animals Act and approved by the animal welfare authorities of Thuringia, Germany (accreditation number: 02-046/14). Transgenic male mice overexpressing human SOD1 with the G93A point mutation (Gurney et al., 1994) ((B6.Cg-Tg(SOD1*G93A) 1Gur/J, JAX Mice stock number 004435)) were obtained from Jackson Laboratory (Bar Harbor, ME, USA) and mated with C57BL/6J females. E13 pregnant mice were sacrificed by cervical dislocation, and the embryos were used for culturing. Mice for ex vivo expression studies were divided into presymptomatic and symptomatic groups by age (8–9 weeks and 19–21 weeks, respectively, for protein expression; 9–10 weeks and 17–21 weeks, respectively, for mRNA comparison). Genotyping was performed as recommended by Jackson Laboratory.

2.2. Motor neuron–enriched cultures

Primary MN cultures were prepared as previously described (Van Den Bosch et al., 2000). Briefly, dissected spinal cord equivalents from nontransgenic and $G93A^{hSOD1}$ embryos were pooled in Hanks' balanced salt solution (Gibco, CA, USA) containing 1% penicillin streptomycin (Gibco, CA, USA) and 1 M 4-(2-hydroxyethyl)-1-piperazineethanesulfonic acid (Roth, Germany). Spinal cord fragments were dissociated into single cells by trypsin digestion (0.1 % trypsin in Hanks' balanced salt solution for 15 minutes at 37 °C) followed by trituration with DNAse (AppliChem, Germany) using fire-polished glass pipettes. MNs and glial cells were separated by 6.2% OptiPrep (Axis-shield Poc AS, Norway) density gradient centrifugation. Glial feeder monolayers were made by seeding astrocytes on Poly-D-lysine hydrobromide–coated (Sigma-Aldrich, USA) 12-mm coverslips (Marienfeld GmbH & Co KG, Germany; 50,000 cells per coverslip). Glial media comprised Dulbecco's modified Eagle's medium/Ham's F-12 medium 1:1 without L-Glutamine (Gibco, UK), 1% penicillin streptomycin (Gibco, UK), and 10% fetal calf serum (PAN Biotech, Germany) for the first week; later on, fetal calf serum was replaced by horse serum (Gibco, UK). Glial proliferation was halted by applying 5 μM arabinofuranosyl cytidine (Calbiochem, Germany) for 24 hours. MNs were seeded on prepared glial feeder layers (15,000-30,000 cells per coverslip). The MN media was composed of neurobasal medium without L-Glutamine (Gibco, UK), 2% 50× B27 Neuromix (Gibco, UK), 0.2% 100× N2 Supplement (Gibco, UK), 1 mM L-Glutamine (Gibco, UK), 2 % horse serum (Gibco, UK), 1% penicillin streptomycin solution (Gibco, UK), and 2 ng/mL human recombinant brain-derived neurotrophic factor (PeproTech, USA). Cells were used for experiments starting from day 13 in vitro.

2.3. Cervical section slice preparation

Mice were anesthetized in cylindrical plexiglas enclosures using isoflurane (Isoflurane-CP, CP-Pharma, Germany). Cervical spinal cord sections for quantitative polymerase chain reaction (qPCR) were extracted from mice after decapitation, frozen, and stored in −80 °C. The mice for immunohistochemical staining were perfused for 2 minutes using phosphate-buffered saline (PBS) followed by a perfusion with buffered 4% refrigerator-cooled paraformaldehyde (PFA, Liquid Production GmbH, Germany). After mice decapitation, the cervical sections were dissected out of their spinal cords. The sections were then incubated in 4% PFA overnight, followed by 10% sucrose overnight incubation, both at 4 °C. Finally, the sections were incubated in 30% sucrose at 4 °C till they sunk. The cervical spinal cord sections were frozen in Tissue-Tek (Sakura, Netherlands) at −20 °C, and slices were prepared using the Leica CM3050S cryostat at −19 °C. The specimens were immobilized on carrier plates using Tissue-Tek (Sakura, Netherlands) during the slicing. Subsequently, 10 slices were directly mounted onto pre-warmed (37° C) SuperFrost Plus (Thermo-Fisher Scientific) glass slides. The slices were stored at −20 °C.

2.4. Immunocytochemistry and CTCF quantification in motor neuron–enriched cultures

After 13 days in vitro, MN-enriched cultures were left untreated (native) or they were treated with 10 μM of calmodulin-dependent protein kinase type II (CAMKII) inhibitor KN-62 (Santa Cruz, TX, USA) and 25 μM MCU activator KMF (Tocris, UK) for 12 hours independently. MN cultures were fixed in 4% PFA. Antigen retrieval for MCU was performed by treating the cells with 1% sodium dodecyl sulfate (Serva, Germany) in PBS for 10 minutes at 37 °C. VDAC staining did not require antigen retrieval. For Cyclophilin D, antigen retrieval was performed by adding heated citrate buffer composed of 10 mM tri-sodium citrate (dihydrate) (Sigma-Aldrich, MO, USA) and 0.05% Tween 20 (Sigma Aldrich, MO, USA) in purified H_2O for 5 minutes. Following a PBS wash, cells were blocked with 10% normal goat serum (NGS) solution (NGS +0.3% Triton X-100 + 3% bovine serum albumin [Serva, Germany] in PBS) for 2 hours at room temperature. Cells were incubated overnight at 4 °C with rabbit anti-MCU (ABIN1988975, 1:100, St. John's laboratory, UK), rabbit anti-VDAC (ab15895, 1:200, Abcam, UK), and rabbit anti-Cyclophilin D (ab64935, 1:100, Abcam, UK) or 1 hour at room temperature with mouse anti-SMI-32 (801701, BioLegend, USA, 1:1000) and anti-βIII tubulin (T2200,1:250, Sigma Aldrich, Germany) primary antibodies in 2% NGS solution. After PBS wash, cells were incubated in secondary antibody solution of Alexa 488 goat anti-rabbit (Invitrogen, CA, USA) for 2 hours (MCU, VDAC, Cyclophilin D) or Alexa 594 goat anti-mouse (Invitrogen, CA, USA) for 1 hour (SMI-32). Secondary antibodies were diluted at 1:200 in 10% NGS solution. Finally, nuclei staining were done with 5 minutes incubation of 4′, 6-diamidino-2-phenylindole (Sigma, MO, USA, 2 μg/mL, room temperature). Specificity of all used antibodies was already demonstrated by other research groups (for details see datasheets). Representative images were taken by the Zeiss laser scanning microscopy (LSM) 710 (Zeiss, Germany) and ZEN 2009 software (Zeiss, Germany). For in vitro expression analysis of cultured MNs, Z-stack images were taken with LSM 510 (Zeiss, Germany) and ZEN 2008 software (Zeiss, Germany). At least 9 different coverslips from 3 distinct preparations and up to 5 to 6 cells per coverslip were imaged and analyzed (1 n = 1 cell). Fluorescence intensity was evaluated using the "z-project" plugin of the Fiji Is Just ImageJ software 2014 (Fiji, open source software based on ImageJ modified by BioVoxxel, Mutterstadt, Germany). The corrected total cell fluorescence (CTCF) of the protein of interest was calculated using formula (Gavet and Pines, 2010): CTCF = Integrated density − (Area of the selected cell × Mean fluorescence of background readings), and it was expressed in arbitrary units.

2.5. Immunohistochemistry and CTCF quantification in cervical section slides

Slides carrying cervical spinal cord sections were transferred into glass cuvettes and dried at 37 °C for 1 h. Sodium citrate dihydrate buffer (pH 6.0) treatment at 100 °C for 20 minutes was done for antigen retrieval. Subsequently, the slices were washed with PBS and blocked with 10% NGS solution for 2 hours at room temperature. Specimen staining was carried out with rabbit anti-MCU (1:100) and mouse anti-SMI-32 (1:500) primary antibodies diluted in 2% NGS. This was followed by 48 hours incubation at 4 °C. After washing with PBS, the slices were stained with secondary antibodies Alexa 488 goat anti-rabbit and Alexa 594 goat anti-mouse diluted at a 1:250 ratio in 10% NGS. 4′,6-diamidino-2-phenylindole was used for 5 minutes for nuclei staining. Thorough wash with PBS was followed by mounting with Fluoromount-G (SouthernBiotech, USA). The specimens were stored at 4 °C protected from light. Representative images and Z-stack images for the ex vivo analysis were made by the Zeiss LSM 710 (Zeiss, Germany) and ZEN 2009 software (Zeiss, Germany). CTCF of MCU was calculated as described previously. Ex vivo data for CTCF calculations were collected from 30 cells per animal (1 n = 1 cell).

2.6. Survival assay

13 days in vitro MN-enriched cultures were treated with KN-62 10 μM (Santa Cruz, TX, USA) and KMF 25 μM alone or in combination with kainate 100 μM (Abcam, UK) for 12 hours. The cells were fixed with 4% PFA and double stained with the neuronal marker βIII-tubulin that stains whole neuronal population, and SMI-32 to specifically stain MNs. All neurons (βIII-tubulin-positive) and MNs (βIII-tubulin-positive and SMI-32-positive) were counted under fluorescence microscope (Axioplan 2 imaging, Zeiss, Germany). The numbers of pretreated neurons were normalized to the numbers of native (nontreated) neurons. Three coverslips from at least 3 different preparations were analyzed (1 n = 1 coverslip).

2.7. Calcium imaging

Measurements of intracellular Ca^{2+} were obtained using the membrane-permeable ester form of the high-affinity ratiometric fluorescent dye fura-2-acetoxymethyl ester (Sigma, Germany). For the Ca^{2+} imaging experiments, spinal neurons were morphologically identified and divided into MNs and non-MNs based on soma diameter (Haastert et al., 2005; Jahn et al., 2006). MN-enriched cultures were incubated in 5–10 μM fura-2-acetoxymethyl ester for 25 minutes in a humidified incubator (5% CO_2) at 37 °C. Following de-esterification at room temperature, the coverslip with the MN-enriched cultures was placed in the recording chamber constantly perfused with a standard extracellular solution containing (in mM): 11.6 4-(2-hydroxyethyl)-1-piperazineethanesulfonic acid, 129.1 NaCl, 5.9 KCl, 11.5 glucose, 1.2 $MgCl_2$, 3.2 $CaCl_2$ and that was pH adjusted to 7.4 with NaOH. Cells were visualized using an upright microscope (Nikon Microscope Eclipse FN1, Tokyo, Japan) with a water immersion objective (NIR Apo, 40x/0.80 W, DIC N2, ∞/0, WD 3.5) (Nikon, Tokyo, Japan). Ratiometric fluorescent images were obtained with the Till Vision Imaging System (Till Photonics, Gräfelfing, Germany). Fura-2 was excited at 350 and 380 nm (Polychrome V, Till Photonics, Gräfelfing, Germany) and the emission light passing the dichroic mirror (DCLP410) and the emission filter (LP440, both obtained from Till Photonics) was collected with a cooled CCD camera (iXON^{EM}+, ANDOR, UK).

Pictures were taken at a frequency of 5 Hz with 5–10 ms exposure time. For the analysis of Ca^{2+} transients, the regions of interest were defined over neuronal soma sparing the nucleus. Cytosolic Ca^{2+} concentration was calculated from recorded ratios at 350/380 nm excitation referring to the formula from Grynkiewicz et al. (1985): $[Ca^{2+}]_{cyt} = KD \times \beta \times (R - R_{min})/(R_{max} - R)$ (Grynkiewicz et al., 1985). Determined constants (KD = 245, β = 3.6 and Rmin = 0.08, Rmax = 0.8) were defined using standard extracellular solution without $CaCl_2$, 2 mM EGTA, and 2 μM ionomycin (Sigma, Germany). R_{max} = 0.8 was determined with the standard extracellular solution containing 30 mM $CaCl_2$ and 10 μM ionomycin (Carriedo et al., 2000). For each experiment, spinal neurons from a minimum of 3 different preparations were recorded (except for Fig. 4D where 2 preparations were recorded, 1 n = 1 cell). Background correction was used during data acquisition. Calcium imaging data processing was with Microsoft Office Excel 2003, 2010 and MATLAB 2015a.

2.8. Quantitative PCR

For in vitro study, cells from 3 coverslips per preparation were pooled together as one sample (1 n = 1 preparation), whereas the ex vivo studies contained whole spinal cords. Total RNA was isolated by the phenol/chloroform extraction method. Spinal cords were lysed using 1 μL of Qiazol Lysis Reagent (Sigma Aldrich, USA) and homogenized using Miccra D1 (Miccra, Germany). For cDNA synthesis, total RNA (500 ng) was transcribed by using the Revert Aid First strand cDNA synthesis kit (Thermo Scientific, USA). qPCR was performed with SYBR Green III Master Mix (Agilent Technologies, USA), as previously described (Jaenisch et al., 2016), by applying the following thermal cycling program: 3 minutes polymerase activation at 95 °C, 40 amplification cycles (95 °C for 10 seconds, 60 °C for 15 seconds), followed by melting curve analysis. The relative expression level of target proteins for every sample in G93A^{hSOD1} cocultures was calculated to the mean value of nontransgenic cocultures using Pfaffl equation (Pfaffl, 2001). Expression of target proteins was normalized to succinate dehydrogenase. Primers (Biomers.net) are listed in Table 1.

2.9. Statistics

The statistical analyses were performed using Sigma Plot 13.0. Data are given as mean ± SEM except for transcriptional data, which are given as mean ± SD. For parametric data, Student's *t*-test was used, for nonparametric, the Mann-Whitney *U*-test was used to compare 2 groups. For multiple comparisons, analysis of variance (ANOVA) (for parametric data) or ANOVA on ranks (for nonparametric data) and two-way ANOVA were used. For ANOVA and ANOVA on ranks, Holm-Sidak and Tukey post hoc tests were used, for two-way ANOVA Dunn's post hoc test for all pairwise multiple comparisons was used. Significance was considered at $p < 0.05$.

3. Results

3.1. Mitochondrial calcium stores are susceptible to the presence of protonophores in embryonic neurons

To verify the influence of mutated hSOD1 on mitochondrial capacity, we measured cytosolic Ca^{2+} while pharmacologically depolarizing mitochondrial membrane potential using 2 different protonophores, 10 μM carbonyl cyanide m-chlorophenyl hydrazone (CCCP, Sigma Aldrich, UK) and 1 μM carbonyl cyanide-4-(trifluoromethoxy)phenylhydrazone (FCCP, Sigma Aldrich). Uptake of Ca^{2+} into mitochondria is dependent on the mitochondrial membrane potential. In the presence of CCCP (Ladewig et al., 2003) and FCCP (Feeney et al., 2003; Wyatt and Buckler, 2004), the pooled mitochondrial Ca^{2+} can be released into the cytosol. The change in the cytosolic Ca^{2+} estimates the mitochondrial Ca^{2+} buffering capacity. 200 μM verapamil (VP) (Sigma, Germany) and 0.5 μM tetrodotoxin (TTX) (Biotrend, Germany) were used in some experiments. VP blocks VGCCs and TTX selectively blocks voltage-gated sodium channels. If the channel blockers were used, the cells were superfused with extracellular solution containing these 2 substances during the whole time of the measurement.

Application of 10 μM CCCP for 100 seconds evoked substantial transient increase of $[Ca^{2+}]_{cyt}$ reaching the maximum peak amplitude within the first 10 seconds of the stimulation. The Ca^{2+} signal was biphasic, consisting of a relatively large and fast initial transient followed by a slower and smaller component continuously decreasing its height until the end of the stimulation. G93A^{hSOD1} MNs showed significantly increased cytosolic Ca^{2+} response $[Ca^{2+}]_{cyt}$, measured as area under the curve (AUC) (n = 18, 11.8 ± 1.2), when compared to nontransgenic MNs (n = 19, 7.7 ± 1, $p < 0.001$, Fig. 1A). Non-MNs from both nontransgenic (n = 32, 6.2 ± 0.5) and G93A^{hSOD1} (n = 43, 5.8 ± 0.4) pool responded similarly without significant differences. However, significant differences between non-MNs and MNs in general in released Ca^{2+} were observed ($p < 0.001$).

Presence of 1 μM FCCP evoked slower increase in $[Ca^{2+}]_{cyt}$ reaching its maximum peak height after 20 seconds and stayed in a plateau phase and slowly decreased its height until the end of the measurement. Application of 1 μM FCCP for 100 seconds did not reveal any significant differences in AUC between nontransgenic (n = 25, 3.8 ± 0.5) and G93A^{hSOD1} (n = 19, 3.8 ± 0.5) non-MNs. However, nontransgenic MNs (n = 29, 5.1 ± 0.6) had significantly increased cytosolic Ca^{2+} response (measured as AUC) when compared to G93A^{hSOD1} MNs (n = 18, 3.5 ± 0.4, $p < 0.05$, Fig. 1B). Once again, significant difference between non-MNs and MNs was apparent ($p < 0.5$). In general, MNs were more susceptible to CCCP and FCCP than non-MNs indicating that MNs particularly depend on mitochondrial Ca^{2+} buffering.

3.2. Caffeine increases releasable mitochondrial calcium in embryonic spinal neurons

Cytosolic Ca^{2+} homeostasis is balanced by the mutual efforts of different organelles within the ERMCC. Moreover, a part of released Ca^{2+} from the ER can be directly taken by the mitochondria. Therefore, not only Ca^{2+} buffering of individual organelles but also mutual interplay of organelles is important. To check the mutual effect of mitochondrial and ER stores on $[Ca^{2+}]_{cyt}$, we used protonophores (CCCP and FCCP) to empty mitochondrial Ca^{2+} stores following the exposure to an induced Ca^{2+} release from the ER (through ryanodine receptors) using caffeine (Sigma Aldrich, USA). Caffeine was applied in pulses (duration: 2 seconds, interpulse interval: 100 seconds) using the protocol described previously in detail by Grosskreutz et al. (2007). 10 μM CCCP was applied for 100 seconds during the repetitive stimulation with 10 mM caffeine, starting 50 seconds before the second caffeine pulse (Fig. 2A). Changes in $[Ca^{2+}]_{cyt}$ were measured as AUC during the time of CCCP application. The first caffeine pulse resulted in a fast cytosolic Ca^{2+} transient indicating functional caffeine-sensitive Ca^{2+} stores in these neurons. As shown before, the Ca^{2+} signal induced by CCCP was biphasic consisting of a relatively large and fast initial transient reaching its first local peak maximum within the first 10 seconds of CCCP stimulation. After the first local maximum, the $[Ca^{2+}]_{cyt}$ decreased for next 10 seconds and then slowly increased until the next caffeine stimulation. Afterward, it reached the absolute curve maximum at the end of the CCCP stimulation. After the washout of CCCP, $[Ca^{2+}]_{cyt}$ started to decrease. Once more, MNs (n = 35, 23.02 ± 0.9) showed significantly increased $[Ca^{2+}]_{cyt}$ load compared to

Table 1
List of primers for qPCR for target proteins

Gene	Primer sequences	Product size
Gapdh	Fwd: CAACAGCAACTCCCACTCTTC Rev: GGTCCAGGGTTTCTTACTCCTT	164 bp
Sdha	Fwd: GGACATCAAGACTGGCAAGGTTAC Rev: ATCAGTAGGAGCGGATAGCAGGAG	107 bp
Mcu	Fwd: ACAACTGCAAGAGGAGGATCGG Rev: TCGAACGCCATCTGGTGAGTAG	64 bp
Micu1	Fwd: TTGACTTGAATGGAGACGGAGAGG Rev: GGAGCGAATGATGCTCTGAACCTG	68 bp
Vdac1	Fwd: GAGTATGGGCTGACGTTTACAG Rev: GAGCTTCAGTCCACGAGCAAG	96 bp
ppif	Fwd: GATGTCGTGCCAAAGACTGCAGAG Rev: TCCTGTGCCATTGTGGTTGGTG	144 bp

Key: qPCR, quantitative polymerase chain reaction.

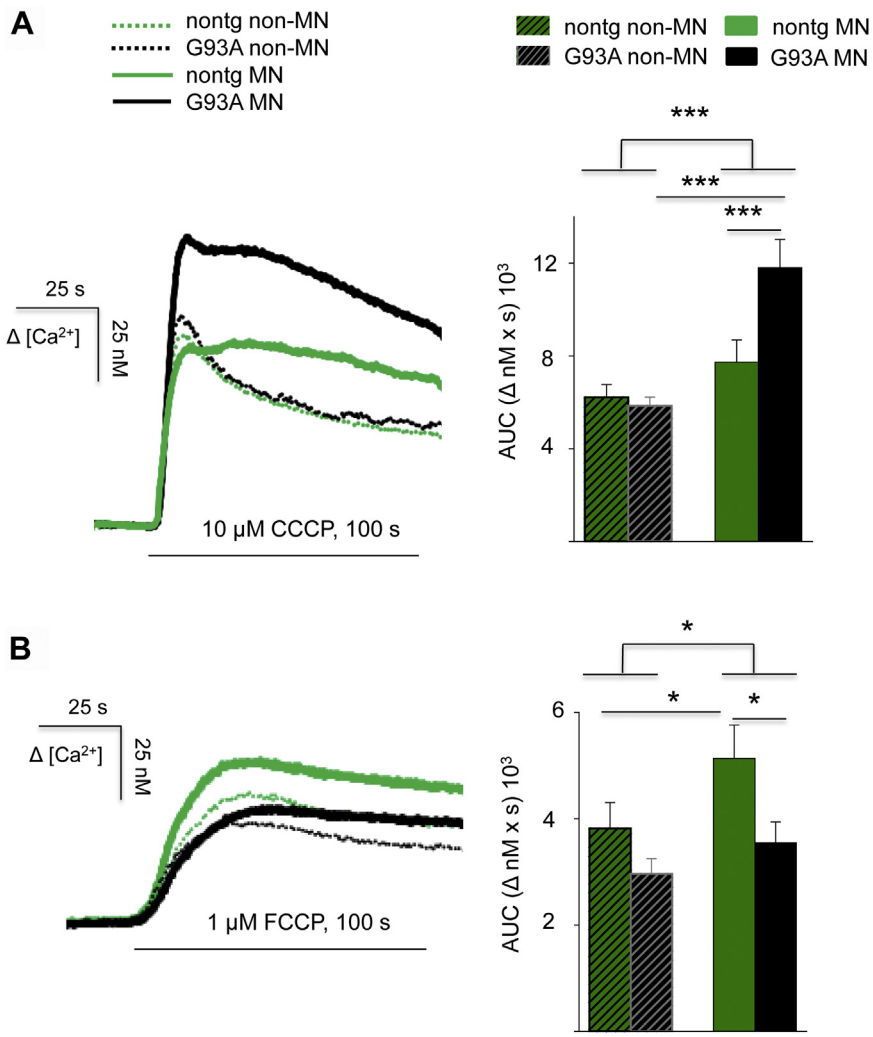

Fig. 1. Evaluation of cytosolic calcium after application of CCCP and FCCP in embryonic spinal neurons (A, B) Protonophores 10 µM CCCP (A) and 1 µM FCCP (B) were applied for 100 seconds. $\Delta[Ca^{2+}]_{cyt}$ levels were measured as area under the curve (AUC). MNs had significantly increased $[Ca^{2+}]_{cyt}$ when compared to non-MNs during the time of protonophore application in both experiments. Application of CCCP (A) resulted in significantly increased $[Ca^{2+}]_{cyt}$ in G93A^{hSOD1} MNs (G93A, n = 18) compared to nontransgenic MNs (nontg, n = 19). On the contrary, application of FCCP (B) resulted in significantly increased response in nontransgenic MNs (n = 29) when compared to G93A^{hSOD1} MNs (n = 18). Two-way ANOVA followed by Holm-Sidak post hoc test. $^{*}p < 0.05$, $^{***}p \leq 0.001$. Abbreviations: ANOVA, analysis of variance; CCCP, carbonyl cyanide m-chlorophenyl hydrazone; FCCP, carbonyl cyanide-4-(trifluoromethoxy)phenylhydrazone; MN, motor neuron.

non-MNs (n = 36, 19.2 ± 1.25, $p < 0.05$, Fig. 2A). Between the genotypes, there was no significant difference seen in non-MNs (nontransgenic: n = 16, 18.8 ± 1.56; G93A^{hSOD1}: n = 20, 19.53 ± 1.9) or MNs (nontransgenic: n = 10, 22.9 ± 1.39; G93A^{hSOD1}: n = 25, 23.05 ± 1.24).

When FCCP was applied in combination with caffeine, continuous rise in $[Ca^{2+}]_{cyt}$ during the whole time of FCCP stimulation was absent. After the initial rise in the presence of FCCP, $[Ca^{2+}]_{cyt}$ stayed in a plateau phase and it slowly decreased until the end of the FCCP application. The second caffeine pulse produced visible Ca^{2+} transient implying that caffeine-induced Ca^{2+} stores were not emptied by the initial caffeine application. Once again, MNs showed (n = 48, 10.8 ± 0.48) significantly increased cytosolic Ca^{2+} load ($p < 0.05$, Fig. 2B) when compared to non-MNs (n = 46, 9.5 ± 0.48, $p < 0.05$). 0.5 µM TTX and 200 µM VP were present in combination with FCCP to minimize possible influx of Ca^{2+} through VGCCs on the plasma membrane.

To confirm that caffeine-induced Ca^{2+} release affects mitochondrial Ca^{2+} stores, we compared the AUC during the time of stimulation (100 seconds) between cells solely treated with protonophores and in combination with caffeine. Short application of caffeine enhanced $[Ca^{2+}]_{cyt}$ increase (CCCP + caffeine: 21.06 ± 0.94; FCCP + caffeine: 9.8 ± 0.42) when compared to cells solely treated with protonophores in non-MNs and MNs from both genotypes (CCCP: 9.47 ± 0.64; FCCP: 5.1 ± 0.47, $p \leq 0.001$, Fig. 2C and D). This finding implies that caffeine increases releasable mitochondrial Ca^{2+}. Once more, we confirmed significant differences between non-MNs and MNs.

3.3. MCU is overexpressed in embryonic G93A^{hSOD1} compared to nontransgenic motor neurons

Disturbances in mitochondrial Ca^{2+} uptake mechanism may be responsible for mitochondrial Ca^{2+} overload in G93A^{hSOD1} MNs. Therefore, we investigated the expression and localization of MCU complex components MCU (pore forming unit), MICU1 (MCU regulating unit), VDAC, and Cyclophilin D (main regulator of the mitochondrial permeability transition pore) in nontransgenic and G93A^{hSOD1} MN cocultures. MNs were stained for SMI-32, a selective MN marker. MCU-positive staining for both nontransgenic and

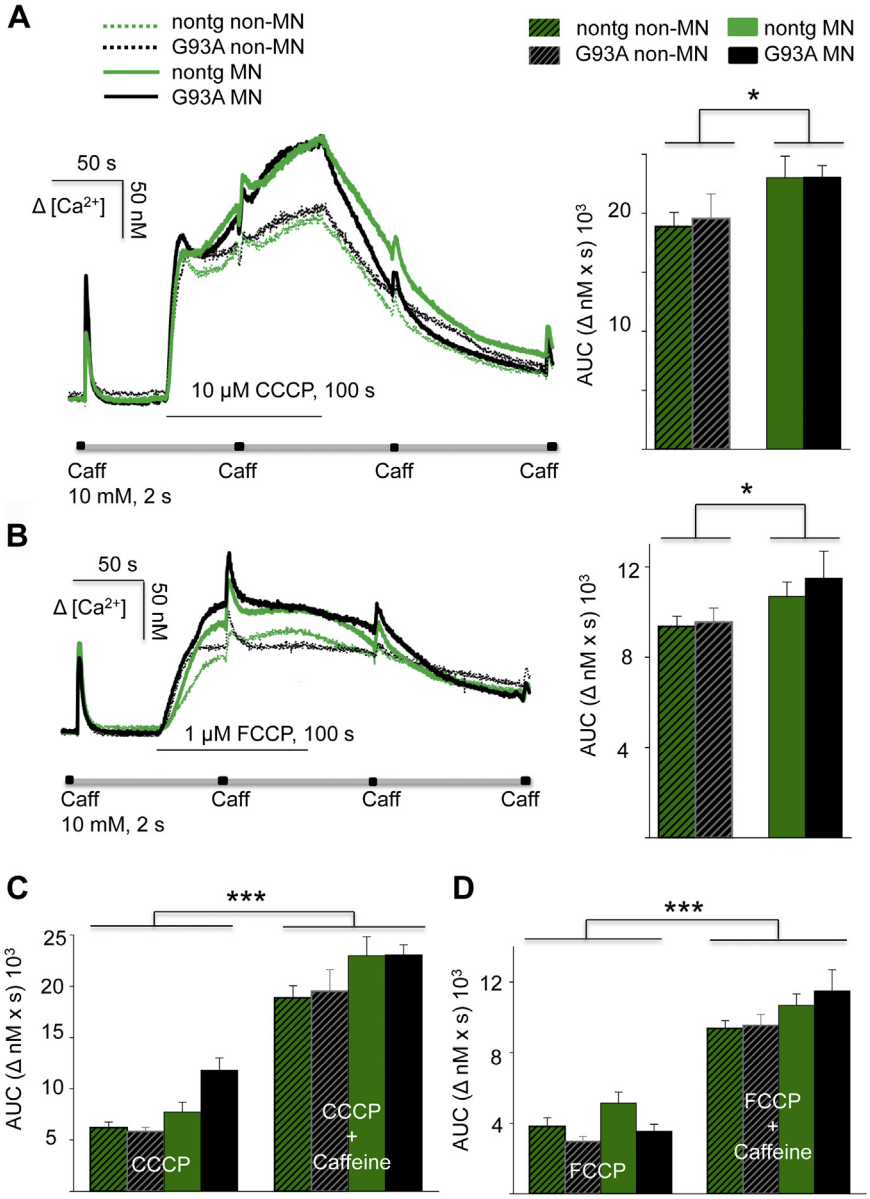

Fig. 2. Evaluation of cytosolic calcium after protonophore and caffeine application in embryonic spinal neurons. (A, B) 10 mM caffeine was applied for 2 seconds every 100 seconds (stimulation indicated by the solid rectangles), producing Ca^{2+} transients. Protonophores CCCP 10 μM (A) and FCCP 1 μM (B) were applied for 100 seconds during repetitive stimulation with caffeine, starting 50 seconds before second caffeine stimulation pulse. Changes in $[Ca^{2+}]_{cyt}$ levels were measured as area under the curve (AUC). Significant differences between non-MNs (CCCP: n = 36; FCCP: n = 46) and MNs (CCCP: n = 35; FCCP: n = 48) have been seen. During experiment B, 0.5 μM tetrodotoxin (TTX) and 200 μM verapamil were present to limit eventual Ca^{2+} influx through VGCCs. Two-way ANOVA followed by Holm-Sidak post hoc test. (C, D) Comparison of AUC during the time of stimulation (100 seconds) between cells solely treated with protonophores and in combination with caffeine. Presence of caffeine significantly increased $[Ca^{2+}]_{cyt}$ when compared to cells solely treated with protonophores in nontransgenic (nontg) and $G93A^{hSOD1}$ (G93A) cells. Two-way ANOVA followed by Holm-Sidak post hoc test. $^{*}p < 0.05$, $^{***}p \leq 0.001$. Abbreviations: ANOVA, analysis of variance; CCCP, carbonyl cyanide m-chlorophenyl hydrazone; FCCP, carbonyl cyanide-4-(trifluoromethoxy)phenylhydrazone; MN, motor neuron.

$G93A^{hSOD1}$ MNs were observed in cell soma, mostly sparing the nucleus, and in the neurites as well. For staining of VDAC, we used an isoform-unspecific antibody because all isoforms are assumed to be present in the nervous system. VDAC was localized in the cell soma, the neurites, and in the nucleus. However, VDAC is not expressed in the nucleus under normal conditions. Cyclophilin D–positive staining was present in the soma and neurites but not in the nucleus of nontransgenic and $G93A^{hSOD1}$ MNs (Fig. 3A).

To investigate mRNA expression, all results were normalized to succinate dehydrogenase. The mRNAs encoding MCU, MICU1, VDAC1, and CyPD (gene *ppif*) were analyzed. Only for MCU, the relative expression levels were significantly higher in $G93A^{hSOD1}$ MN cocultures (n = 6, 1.21 ± 0.08) in comparison to nontransgenic cocultures (n = 6, 1.0 ± 0.06, $p < 0.05$, Fig. 3B). We also used CTCF value to quantify immunofluorescence staining of mitochondrial proteins specifically in MNs. Once again, only CTCF value of MCU in $G93A^{hSOD1}$ genotype was significantly increased (n = 53, 3.69 ± 0.34) when compared to nontransgenic MNs (n = 56, 2.57 ± 0.19, $p < 0.5$, Fig. 3C).

3.4. Mitochondrial Ca^{2+} uptake influences spontaneous Ca^{2+} activity in embryonic spinal neurons

Activators of the MCU allow direct testing of the influence of mitochondrial Ca^{2+} uptake on the intracellular Ca^{2+} homeostasis

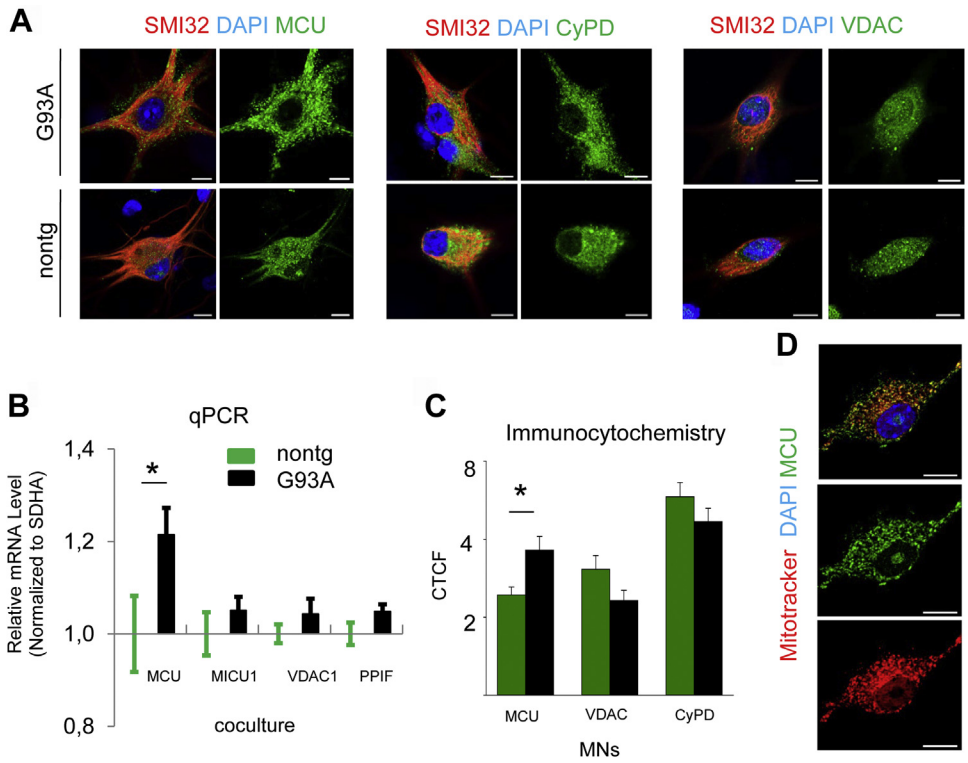

Fig. 3. MCU is overexpressed in embryonic G93A^{hSOD1} motor neurons relative to nontransgenic motor neurons. (A) Representative pictures of MCU, VDAC, and CyPD staining are shown in green in nontransgenic (nontg) and G93A^{hSOD1} (G93A) neurons. Nuclei (blue) were stained by DAPI and MNs were identified by SMI-32R (red). Scale bar = 10 μm. (B) The relative expression of MCU, MICU1, VDAC1, and CyPD (gene *ppif*) is normalized to SDHA for nontransgenic (nontg) and G93A^{hSOD1} (G93A) samples. Only MCU shows a significantly higher expression in G93A^{hSOD1} cultures compared to nontransgenic cultures (n = 6 in both groups). (C) Protein expression is measured by immunocytochemistry as CTCF. CTCF of MCU in G93A^{hSOD1} MNs (n = 53) was significantly increased when compared to nontransgenic MNs (n = 56). Mann-Whitney-*U* Test. *$p < 0.05$. (D) Mitotracker (red) was used to show overlapping of MCU with mitotracker stained mitochondria. Scale bar = 10 μm. Abbreviations: CTCF, corrected total cell fluorescence; CyPD, cyclophilin D; DAPI, 4′,6-diamidino-2-phenylindole; MCU, mitochondrial calcium uniporter; MICU, mitochondrial calcium uptake 1; MN, motor neuron; qPCR, quantitative polymerase chain reaction; VDAC, voltage-dependent anion channel. (For interpretation of the references to color in this figure legend, the reader is referred to the Web version of this article.)

of the cell. Here, we used the MCU opener KMF to examine its effect on $[Ca^{2+}]_{cyt}$ (Fig. 4A). KMF 50 μM significantly increased the number of cytosolic Ca^{2+} transients in nontransgenic non-MNs (n = 16, no stimulation: 1.19 ± 0.32, KMF: 5.94 ± 0.92, KMF + VP + TTX: 0.375 ± 0.13, $p < 0.001$) and in MNs (n = 17, no stimulation: 1.59 ± 0.49, KMF: 7 ± 0.91, KMF + VP + TTX: 0.29 ± 0.11, $p < 0.01$, $p < 0.001$; Fig. 4B). Same effect was also observed in G93A^{hSOD1} non-MNs (n = 32, no stimulation: 1.38 ± 0.36, KMF: 2.72 ± 0.45, KMF + VP + TTX: 0.09 ± 0.05, $p < 0.01$, $p < 0.001$) and MNs (n = 13, no stimulation: 1.07 ± 0.49, KMF: 2.31 ± 0.38, KMF + VP + TTX: 0.15 ± 0.1, $p < 0.01$, $p < 0.001$, Fig. 4B). However, no difference between non-MNs and MNs was observed. When VP and TTX were applied together with KMF, the number of Ca^{2+} transients significantly reduced in all groups implying that these Ca^{2+} oscillations are dependent or enhanced by extracellular Ca^{2+} entry. Furthermore, in G93A^{hSOD1} neurons most transients appeared in the first minute of KMF application, whereas in nontransgenic neurons most transients appeared in the second minute of KMF stimulation (Fig. 4C). These results suggest that presence of spontaneous Ca^{2+} activity is directly related to the ability of mitochondria to take up Ca^{2+}. Second, different transient pattern observed in G93A^{hSOD1} neurons may be the consequence of changed MCU expression and function seen in embryonic G93A^{hSOD1} neurons.

To confirm that KMF-induced Ca^{2+} transients are indeed reduced in the presence of VP and TTX, different stimulation protocol was performed (Fig. 4D). KMF produced changes in $[Ca^{2+}]_{cyt}$, however, Ca^{2+} transients (shaped as peaks seen in Fig. 4A) were absent.

3.5. KN-62 protects G93A^{hSOD1} embryonic motor neurons against kainate-induced excitotoxicity

Because glutamate-induced neuronal death requires mitochondrial Ca^{2+} uptake (Stout et al., 1998), we challenged our cocultures with the selective AMPAR agonist kainate to induce excitotoxicity (Lautenschlager et al., 2013) and tested pharmacological manipulation of MCU as a possible rescue strategy. Therefore, we used (1) KN-62 as a selective CAMKII inhibitor that is known to be increased in G93A mice (Chang and Martin, 2016, Hu et al., 2003b) and can upregulate MCU activity (Joiner et al., 2012) and (2) KMF as an MCU activator. The cultures were treated for 12 hours with 100 μM kainate, 10 μM KN-62, and 25 μM KMF alone or kainate in combination with one of the drugs. KN-62 or KMF did not show a toxic effect on the survival of nontransgenic (native: n = 11, 1 ± 0.2; KN-62: n = 9, 1.19 ± 0.26; KMF: n = 12, 1.17 ± 0.34) or G93A^{hSOD1} non-MNs (native: n = 12, 1 ± 0.13; KN-62: n = 11, 0.74 ± 0.17; KMF: n = 12, 0.88 ± 0.13) or nontransgenic (native: n = 11, 1 ± 0.2; KN 62: n = 9, 0.86 ± 0.18; KMF: n = 12, 1.24 ± 0.28) or G93A^{hSOD1} MNs (native: n = 12, 1 ± 0.12; KN-62: n = 11, 0.82 ± 0.18; KMF: n = 12, 0.82 ± 0.17) when compared to native (Fig. 5A and B). 50% of nontransgenic (n = 12, $p = 0.058$) and 27% of G93A^{hSOD1} (n = 12, $p < 0.01$) non-MNs survived in the presence of kainate, and 20% of nontransgenic (n = 12, $p \leq 0.001$) and 9% of G93A^{hSOD1} (n = 12, $p \leq 0.001$) MNs survived. These differences confirm the selective vulnerability of MNs, especially in G93A^{hSOD1} genotype. KN-62 protected G93A^{hSOD1} MNs against kainate, as shown by the increase in MN survival by 13% (n = 11, $p < 0.01$,

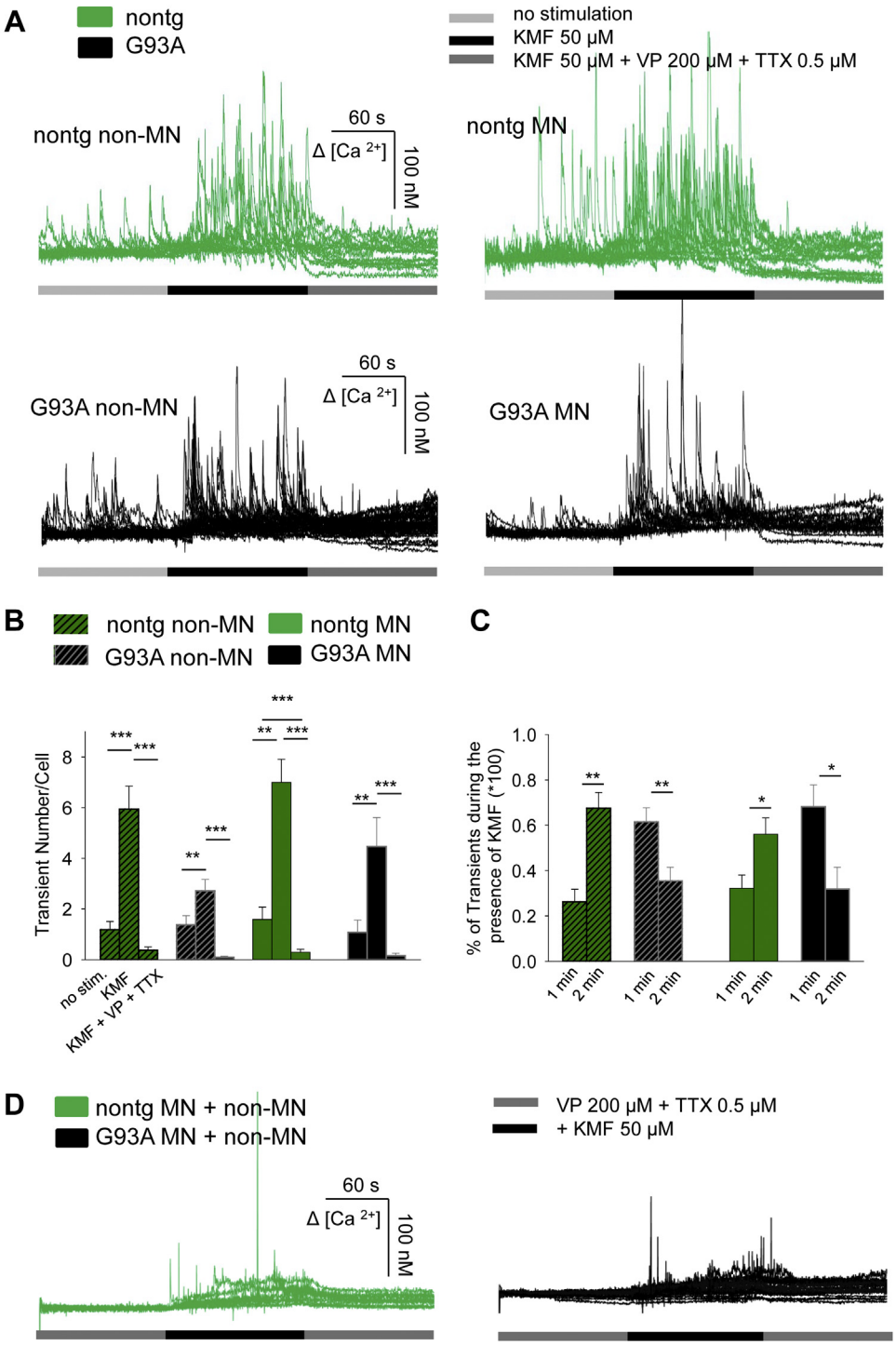

Fig. 4. Kaempferol increases spontaneous Ca^{2+} activity in embryonic spinal neurons. (A) Transients of spontaneous Ca^{2+} activity are presented, first 2 minutes without stimulation, followed by 2 minutes of stimulation with 50 µM of kaempferol (KMF) and 2 minutes of 50 µM kaempferol +200 µM VP (VP) and 0.5 mM tetrodotoxin (TTX). (B) Number of transients during kaempferol presence show increased spontaneous Ca^{2+} activity in nontransgenic (nontg) non-MNs (n = 16) and MNs (n = 17) and as well in $G93A^{hSOD1}$ (G93A) non-MNs (n = 32) and MNs (n = 13). Application of VP and TTX significantly reduced Ca^{2+} transients in all 4 recorded groups. One-way ANOVA on ranks followed by post hoc Tukey's test. (C) In nontransgenic neurons, most Ca^{2+} transients appeared in the second minute of KMF stimulation, whereas in $G93A^{hSOD1}$ neurons most transients appeared during the first minute of KMF stimulation. Mann-Whitney-*U* test. (D) Traces of Ca^{2+} activity are presented, first 2 minutes with the presence of VP and TTX, followed by 2 minutes of stimulation with 50 µM of kaempferol (KMF) + 200 µM VP + 0.5 µM TTX, and 2 minutes with the presence of VP and TTX. Kaempferol produced changes in $[Ca^{2+}]_{cyt}$, however, Ca^{2+} transients (shaped as peaks seen in Fig. 4A) were absent in nontransgenic (n = 22) and $G93A^{hSOD1}$ (n = 12) genotype. $^{*}p < 0.05$, $^{**}p < 0.01$, $^{***}p \leq 0.001$. Abbreviation: ANOVA, analysis of variance.

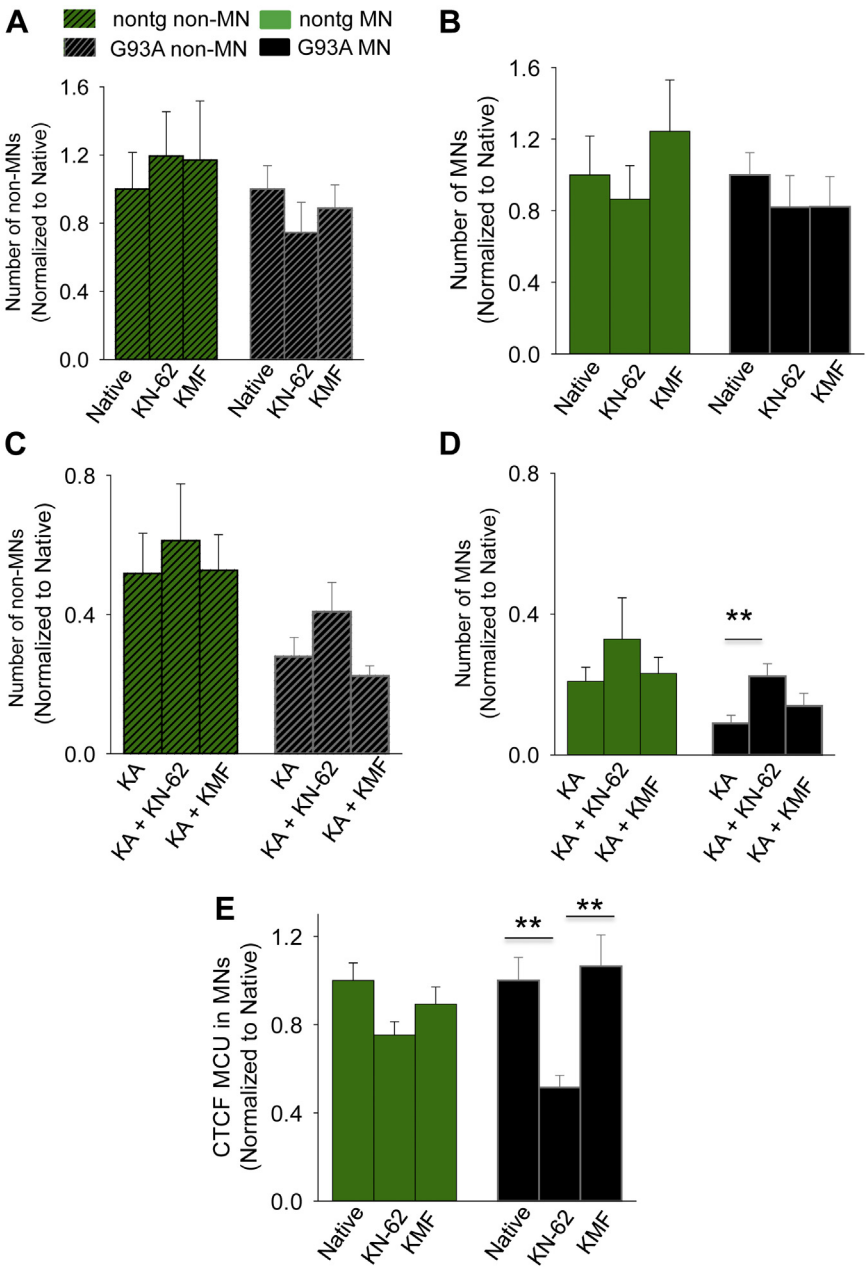

Fig. 5. Pharmacological manipulation of MCU protects motor neurons against kainate-induced excitotoxicity in embryonic G93A^{hSOD1} motor neurons. Embryonic MN cultures from nontransgenic (nontg) and G93A^{hSOD1} (G93A) mice were treated for 12 hours with the following substances: 100 μM kainate (KA), 10 μM KN-62, and 25 μM kaempferol (KMF) alone or in combination. Three coverslips per at least 3 different preparations were analyzed (minimum of n = 9 coverslips from 3 independent experiments). (A, B) KN-62 or KMF did not show a toxic effect on the survival of non-MNs (A) or MNs (B) when compared to native (nontreated controls) for both nontransgenic and G93A^{hSOD1} genotype (nontg native: n = 11, KN-62: n = 9, KMF: n = 12; G93A native: n = 12, KN-62: n = 11, KMF: n = 12). (C, D) No rescue effect against kainate has been seen in non-MNs by addition of KN-62 or KMF (C). Significant rescue effect of KN-62 against kainate-induced excitotoxicity has been seen in G93A^{hSOD1} MNs but not in nontransgenic MNs (D) (nontg KA: n = 12, KA + KN-62: n = 9, KA + KMF: n = 12; G93A native: n = 12, KN-62: n = 11, KMF: n = 12). (E) MNs cocultures were treated with 10 μM KN-62 and 25 μM KMF for 12 hours (up to 5 cells per coverslip from minimum 11 coverslips and 4 independent experiments were analyzed, n = 50 to 60 cells). Although KN-62 significantly decreased MCU protein expression (as measured by immunocytochemistry as CTCF) in G93A^{hSOD1} (G93A) MNs, it did not have the same effect in nontransgenic MNs (nontg native: n = 60, KN-62: n = 60, KMF: n = 50; G93A native: n = 59, KN-62: n = 60, KMF: n = 60). One-way ANOVA (for A, B, and C). ANOVA on ranks following Dunn's method for all pairwise multiple comparison (for D, E). $^{**}p < 0.01$. Abbreviations: ANOVA, analysis of variance; MCU, mitochondrial calcium uniporter.

Fig. 5D). MCU activation by KMF did not show significant protective effect (Fig. 5D). We confirmed stronger susceptibility of MNs toward kainate-induced AMPAR-mediated excitotoxicity (Benyamin et al., 2014; Van Den Bosch et al., 2000), with higher death rate in G93A^{hSOD1} MNs which were rescued by KN-62.

3.6. Protective effect of KN-62 involves reduction of MCU expression

MCU knockdown was shown to be neuroprotective against glutamate excitotoxicity (Qiu et al., 2013). Because KN-62 was protective against kainate-induced excitotoxicity and KMF increased spontaneous Ca^{2+} activity in G93A^{hSOD1} MNs, we

examined if these compounds affect MCU expression (measured by immunocytochemistry as CTCF). G93A^{hSOD1} and nontransgenic cocultures were treated with 10 μM KN-62 and 25 μM KMF (lower concentration for long-term experiment) for 12 h. CTCF values of MCU in MNs were calculated and compared to control (non-treated). In nontransgenic MNs, CTCF of MCU was moderately decreased in KN-62–treated MNs (n = 60, 0.85 ± 0.06) when compared to native (n = 60, 1 ± 0.05). However, KMF did not affect CTCF of MCU (n = 50, 0.99 ± 0.06) in nontransgenic MNs (Fig. 5E). In G93A^{hSOD1} MNs, KN-62 significantly decreased CTCF of MCU (n = 60, 0.54 ± 0.05) when compared to native (n = 59, 1 ± 0.1, $p <$ 0.01). Similar to nontransgenic MNs, KMF did not significantly affect CTCF of MCU in G93A^{hSOD1} MNs (n = 60, 1.01 ± 0.1, Fig. 5E). Taken together, KN-62 reduced MCU expression, specifically in G93A^{hSOD1} MNs.

3.7. MCU expression increases with age in postnatal mice and is reduced in G93A^{hSOD1} genotype compared to nontransgenic mice

Next, we examined the expression of the MCU protein ex vivo. The postnatal mice were used to approximate the conditions and environment of the diseased MNs as much as possible to that of processes developing in human patients. MCU protein expression was investigated by immunohistochemistry (Fig. 6A) as CTCF

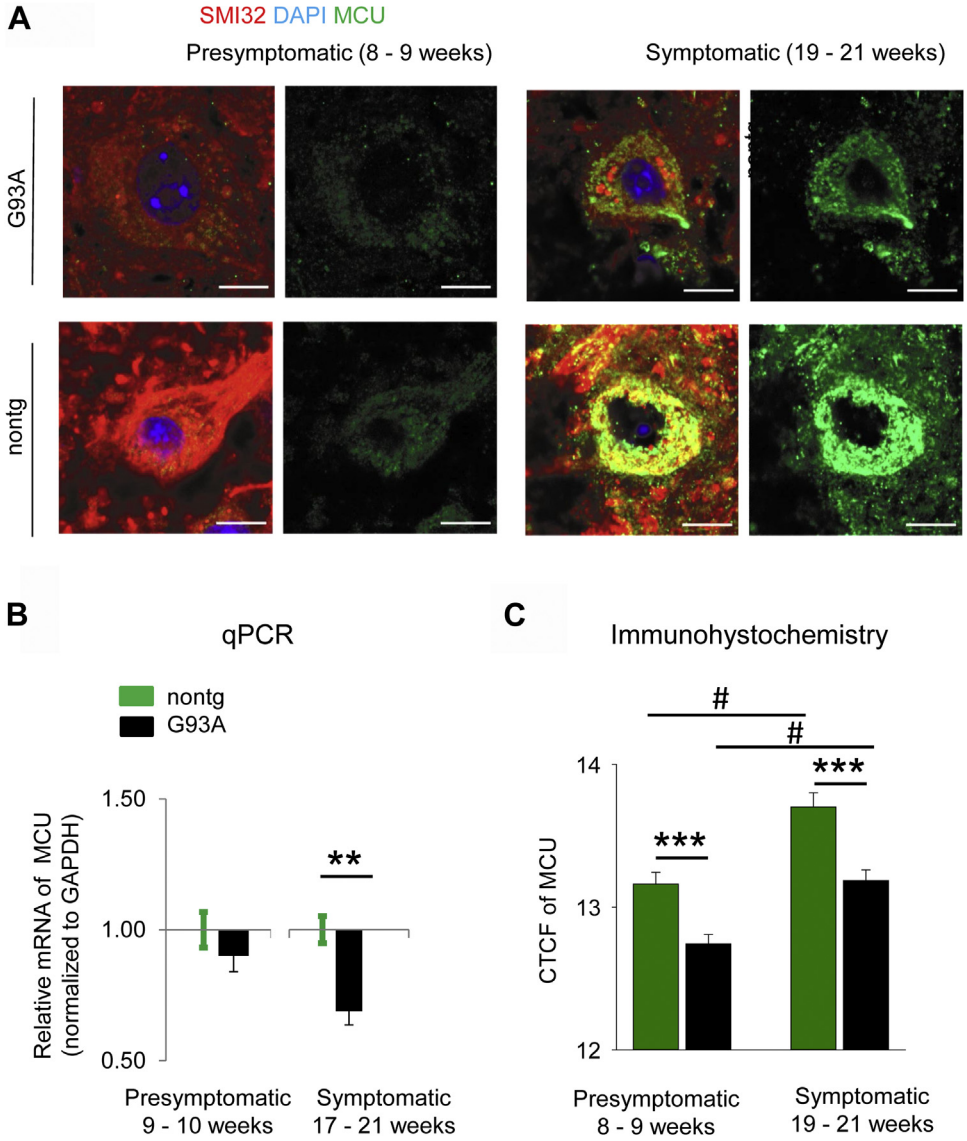

Fig. 6. MCU mRNA and MCU protein expression are decreased in symptomatic G93A^{hSOD1} mice. (A) Images displayed represent single-plane LSM scans of MNs in anterior horn gray matter of the cervical spinal cord section of adult nontransgenic and G93A^{hSOD1} mice. MCU channel (green) reflects the MCU protein expression in nontransgenic (nontg) and G93A^{hSOD1} (G93A) mice in 2 age groups (8–9 weeks and 19–21 weeks old). Motor neurons were identified using SMI-32 (red). Nuclei are shown by DAPI (blue). Scale bar = 10 μm. (B) MCU mRNA is decreased in mouse cervical spinal cord sections of symptomatic G93A^{hSOD1} (n = 7, 17–21 weeks) mice when compared to age-matched nontransgenic controls (n = 5). MCU mRNA levels were not significantly different in presymptomatic G93A^{hSOD1} mice (n = 6, 8–9 weeks) when compared to age-matched controls (n = 3). Student's *t*-test. (C) MCU protein expression was measured by immunohistochemistry as CTCF (AU). MCU CTCF was significantly decreased in symptomatic (n = 30 from 3 mice, 19–21 weeks) and presymptomatic (n = 30 from 3 mice, 9–10 weeks) G93A^{hSOD1} mice when compared to age-matched nontransgenic controls (n = 150 from 5 mice, n = 150 from 5 mice). MCU expression significantly increased with the animal age in nontg and in G93A genotype (indicated by #). Two-way ANOVA followed by Holm-Sidak post hoc test. $^{**}p < 0.01$, $^{***}p \leq$ 0.001, $\#p \leq 0.001$. Abbreviations: ANOVA, analysis of variance; CTCF, corrected total cell fluorescence; DAPI, 4′,6-diamidino-2-phenylindole; GAPDH, glyceraldehyde 3-phosphate dehydrogenase; LSM, laser scanning microscopy; MCU, mitochondrial calcium uniporter. (For interpretation of the references to color in this figure legend, the reader is referred to the Web version of this article.)

(Fig. 6C). We found that MCU protein expression increases with the mice age in G93A^{hSOD1} mice (8–9 weeks old/presymptomatic: n = 150 cells from 5 mice, 12.74 ± 0.07; 19–21/symptomatic weeks old: n = 5 cells from 5 mice, 13.18 ± 0.07, $p < 0.001$) and in aged-matched nontransgenic controls (8–9 weeks old: n = 90 from 3 mice, 13.16 ± 0.08; 19–21 week old: n = 90 from 3 mice, 13.7 ± 0.09, $p < 0.001$, Fig. 6C). We have also shown that the MCU protein expression is notably decreased in G93A^{hSOD1} mice when compared to nontransgenic mice in both disease stage groups ($p < 0.001$, Fig. 6C). Investigation of MCU mRNA by qPCR showed significantly increased MCU mRNA levels in nontransgenic mice, albeit only when comparing the 19- to 21-week-old age group (G93A^{hSOD1}: n = 7, 0.68 ± 0.05; nontransgenic: n = 5, 1 ± 0.05, $p < 0.01$, Fig. 6B).

4. Discussion

Calcium is crucial for normal cellular functioning. However, prolonged exposure to increased levels of highly reactive Ca^{2+} is cytotoxic. Ongoing clinical trials show that excitotoxicity and mitochondrial dysfunction are appealing targets for intervention in treatment of ALS (Tadic et al., 2014).

4.1. Motor neurons depend on mitochondrial Ca^{2+} buffering

As action potential Ca^{2+} oscillations in MNs occur at high frequencies of up to 10 Hz (Lips and Keller, 1999; Palecek et al., 1999), rapid recovery of Ca^{2+} transients is necessary to mediate proper physiological functions. It is believed that the fast modulation in MNs is achieved through low levels of Ca^{2+} binding proteins (Alexianu et al., 1994) and consequent higher dependency on mitochondria for fast Ca^{2+} buffering (Grosskreutz et al., 2007; Lautenschlager et al., 2013). Under conditions of prolonged $[Ca^{2+}]_{cyt}$ elevations, mitochondrial Ca^{2+} uptake can increase 10- to 1000-fold (Williams et al., 2013). However, following repetitive AMPAR stimulation, fast buffering processes are overwhelmed in MNs, unlike that seen in non-MNs (Grosskreutz et al., 2007).

Given that we observed significant differences between MNs and non-MNs in the presence of protonophores, we assume that mitochondria undertake the lion's share of Ca^{2+} buffering in MNs. In the present study, the application of the protonophores shows somewhat different results for nontransgenic and G93A^{hSOD1} MNs. In the CCCP protocol, G93A^{hSOD1} MNs appear to result in higher $[Ca^{2+}]_{cyt}$, whereas in the FCCP protocol, nontransgenic MNs seem to have a higher increase of $[Ca^{2+}]_{cyt}$. Initial cytosolic Ca^{2+} increase observed in the presence of FCCP was not as steep as that seen after CCCP application. The maximum cytosolic Ca^{2+} rise occurred later than it did with CCCP, indicating that FCCP potentially acts on organelles at a greater distance from the plasma membrane (such as mitochondria). Furthermore, FCCP does not affect the plasma membrane potential in MNs indicating its specificity to the mitochondrial membrane depolarization (Ladewig et al., 2003). In contrast to CCCP, FCCP was more precise and specific in terms of being able to exert disturbances in the mitochondrial membrane potential. Thus, as FCCP released less Ca^{2+} in the G93A^{hSOD1} MNs, it would appear that the G93A^{hSOD1} mutation profoundly reduces mitochondrial Ca^{2+} buffering in MNs. A similar observation using FCCP was reported by Jaiswal et al. (2009) in G93A-transfected SH-SY5Y neuroblastoma cells (Jaiswal et al., 2009).

Given that $[Ca^{2+}]_{cyt}$ was significantly increased when caffeine was applied before protonophores, it seems that caffeine additionally loaded Ca^{2+} into mitochondria. However, differences between the genotypes were absent probably because massive $[Ca^{2+}]_{cyt}$ increase masked previously observed differences. This finding supports the premise that mitochondria represent an important buffering system in spinal neurons, probably not only by taking Ca^{2+} from the cytosol but also by coupling with other intracellular Ca^{2+} stores.

4.2. MCU as a target against excitotoxicity

Hyperexcitability is a long-standing phenomenon in the ALS pathogenic framework. If we were to consider this concept, ALS displays a markedly unique phenomenon of hyperexcitability that influences the motor system, as indicated by symptoms such as fasciculations, spasticity, muscle cramps, and hyper-reflexia that are almost always experienced during the ALS disease course (Bae et al., 2013).

KN-62 protected G93A^{hSOD1} MNs from kainate-induced excitotoxicity in embryonic cultures. This protection by KN-62 may be mediated by an indirect decrease in MCU as KN-62 significantly decreased the MCU expression in G93A^{hSOD1} MNs, which again suggests existence of coupled processes inside the ERMCC. Potentially, a therapeutic strategy could then result in a drop in the early upregulation of MCU. Elevated cytosolic Ca^{2+} from excitotoxic Ca^{2+} influx might activate CAMKII that consequently leads to MCU overexpression (Qiu et al., 2013). Studies on hyperexcitability and excitotoxicity in the early pathogenesis of ALS mostly demonstrate intracellular mitochondrial overload due to increased Ca^{2+} influx through AMPARs. However, Ca^{2+} influx driven by increased VGCCs expression (Chang and Martin, 2016) may also increase protein kinase activation in mouse models and patients with ALS (Krieger et al., 1996). Furthermore, CAMKII was increased in G93A^{hSOD1} MNs and patients with ALS (Hu et al., 2003a,b). Pharmacological agents that directly block MCU have already been used, such as the hexavalent cation ruthenium red and its derivative Ru360. Ruthenium red can selectively block the uniporter in isolated mitochondria but also has a nonselective effect on certain plasma membrane ion channels of many cell types (Hajnoczky et al., 2006). Ru360 appears to be more specific, but its instability in aqueous solutions limits its application (Lautenschlager et al., 2013).

Acute pharmacological activation of MCU by KMF increased Ca^{2+} oscillations, which were diminished when VGCCs were blocked, indicating that they are enhanced by extracellular Ca^{2+} influx. Thus, we propose that mitochondrial Ca^{2+} uptake modulates spontaneous cytosolic Ca^{2+} activity by coupling with Ca^{2+} channels on the plasma membrane. Moreover, the patterns of KMF-induced Ca^{2+} transients were specifically changed in G93A^{hSOD1} genotype, suggesting the destructive action of G93A^{hSOD1} in mitochondrial Ca^{2+} handling. However, chronic presence of KMF neither harmed the MNs nor changed the MCU expression. MNs seem to adapt to chronic KMF presence because there was no influence on MN survival. KMF serves as a fine tool to acutely study MCU-dependent cytosolic Ca^{2+} changes, however, its role in studying changes in MCU expression and MN survival are limited.

Fuchs et al. (2013) did not observe changes in excitability or elevated mitochondrial Ca^{2+} uptake during the end stage of the disease in G93A^{hSOD1} mice; instead, they demonstrated a reduction in mitochondrial Ca^{2+} uptake. They postulated a complete remodeling of Ca^{2+} handling during ALS progression that ranged from mitochondrial uptake to mitochondrial uptake failure and enhanced plasma membrane extrusion during the end stages (Fuchs et al., 2013), which our data from adult animals also support. In comparison to the nontransgenic genotype, an overexpression of MCU in cultured G93A^{hSOD1} embryonic MNs was followed by a "switch" to MCU downregulation in presymptomatic and symptomatic adult G93A^{hSOD1} mice. It has been reported that neurons display up to 67% larger mean Ca^{2+} currents in the embryonic versus postnatal stage, owing to increased growth and

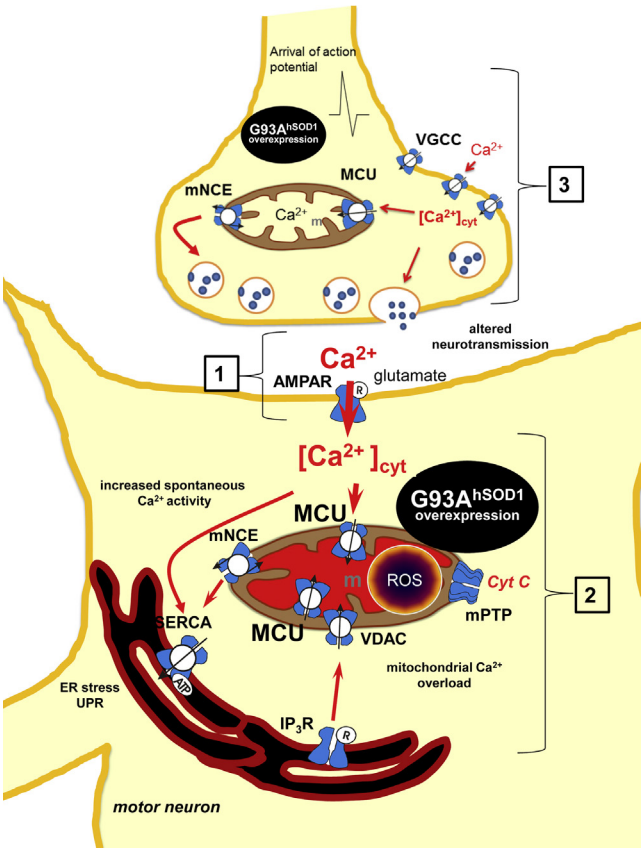

Fig. 7. Targeting mitochondrial Ca^{2+} uptake within G93A^{hSOD1} model. The illustration summarizes MN injury within the ER mitochondrial Ca^{2+} cycle in ALS. (1) Over-stimulated AMPARs allow excessive Ca^{2+} entry, which results in toxic shift of Ca^{2+} from the ER to the mitochondria (m). (2) Disbalance in Ca^{2+} homeostasis cause abnormal ROS generation. Together, these pathways result in reduced production of ATP, depolarization of the mitochondrial membrane potential, and opening of the mPTP channel with release of cytochrome c (CytC) and downstream activation of apoptosis. (3) Furthermore, diseased synaptic mitochondria affect synaptic transmission and organization of neurotransmitter vesicle pools probably even enhancing ALS-specific glutamate excitotoxicity. Thus, we suggest that uptake of Ca^{2+} into the diseased mitochondria may directly alter spontaneous Ca^{2+} activity. In sum, pathophysiological processes within the G93A^{hSOD1} model are probably all coupled and accelerate each other. Pharmacological manipulation of MCU function and MCU expression may be a neuroprotective strategy against excitotoxicity in ALS. Abbreviations: AMPAR, α-amino-3-hydroxy-5-methyl-4-isoxazolepropionic acid receptor; ALS, amyotrophic lateral sclerosis; ER, endoplasmic reticulum; IP3R, inositol 1,4,5-trisphosphate receptor; MN, motor neuron; mPTP, mitochondrial permeability transition pore; mNCE, mitochondrial Na+/Ca2+ exchanger; SERCA, sarcoplasmic/endoplasmic reticulum Ca2+-ATPase; VDAC, voltage-dependent anion channel; VGCC, voltage-gated calcium channel; UPR, unfolded protein response.

development (Collings et al., 1999). During the embryonic development period, MNs have been shown to produce an increased expression of AMPAR and a high Ca^{2+} influx in comparison to other neurons (Van Den Bosch et al., 2000). Kainate-stimulated mice embryonic G93A^{hSOD1} MNs displayed a reduced clearance of Ca^{2+} from the cytosol when compared to nontransgenic MNs (Lautenschlager et al., 2013). Taking this into account, increased MCU expression in embryonic G93A^{hSOD1} MNs is required for buffering large Ca^{2+} currents. However, at a presymptomatic postnatal stage, this buffering activity is most likely not required at this extent, as the Ca^{2+} influx that would support the intense developmental enzymatic and signaling activity are no longer required (Collings et al., 1999). Possibly, MCU is upregulated in response to the initial Ca^{2+}-derived excitotoxicity and subsequently "burns out" as ALS progresses. On the other hand, the reduction in MCU expression in presymptomatic postnatal G93A^{hSOD1} MNs when compared to age-matched controls could stem from an attempt by the cells to protect themselves from excessive Ca^{2+} loads as they are necessary for glutamate-induced excitotoxic death (Stout et al., 1998). A prolonged repeated Ca^{2+} loading at the rate present in the embryonic G93A^{hSOD1} MNs could be detrimental to postnatal presymptomatic MN integrity when combined with the embryonic MN MCU expression. As previously mentioned, an epigenetic switch could induce this protective behavior of the MNs.

Contrary to our results, a previous study on transcriptome-level analysis of hypoglossal MNs from G93A^{hSOD1} mice identified specific upregulation of the MCU and interestingly demonstrated the upregulation of plasmalemmal Ca^{2+} transporters (Muhling et al., 2014). However, expression was not investigated at the proteomic level, thus limiting the inferences that can be drawn from these data. MCU knockdown to protect hippocampal and cortical neurons against NMDAR-induced excitotoxicity was also reported and overexpression of MCU increased mitochondrial Ca^{2+} leading to excitotoxic cell death (Qiu et al., 2013).

In summary, we can infer that neuroprotective mechanisms to counter the high Ca^{2+} influx primarily act by upregulating the MCU in G93A^{hSOD1} genotype. This, however, is a provisional solution, as prolonged upregulation would ultimately result in increased reactive oxygen species and reduced adenosine triphosphate production. It is plausible that the ERMCC continues to adapt and reduces MCU expression to help cope with this overload, but ultimately the distressed MNs succumb (Fig. 7). We recommend that future studies also use the analyses of the size and number of mitochondria in addition to MCU analyses. It is crucial to understand if and how changes in MCU function and expression depend on possible changes in size and number of mitochondria themselves. Moreover, in this study, the objective was only to compare symptomatic and nonsymptomatic mice. Age-dependent analysis of MCU expression can, also, be carried out in future studies to have a better understanding of the expression trajectory in G93A^{hSOD1} mouse MNs.

5. Conclusion

We demonstrated that KMF-induced cytosolic Ca^{2+} activity is altered by the presence of mutated hSOD1. Given that mitochondrial Ca^{2+} dynamics regulate neurotransmission, disturbances in cytosolic Ca^{2+} homeostasis in G93A^{hSOD1} MNs may be direct consequence of altered mitochondrial function at synapses. Interestingly, long-term exposure to KMF did not affect MN survival or impact MCU expression, indicating that MNs have the capacity to dynamically adjust their Ca^{2+} buffering systems depending on their environment. We also showed that KN-62 protects MNs from kainate-induced excitotoxicity possibly by downregulating MCU expression. Pathophysiological processes associated with ERMCC breakdown are coupled and exacerbate each other. Therefore, it is possible that using targeted interventions specific for single components like the MCU might help alleviate stress within the ERMCC, thereby improving MN survival in ALS.

Disclosure

The authors have no conflicts of interest to disclose.

Acknowledgements

This research is supported by BMBF, Germany (Bundesministerium für Bildung and Forschung) in the framework of the E-RARE program (PYRAMID, 01GM1304) and JPND (SOPHIA,

01ED1202B) of the European Union to JG and the Deutsche Gesellschaft für Muskelkranke e.V. (DGM) in collaboration with the German Network for Motoneuron Disease (MND-NET). Furthermore, it is supported by an ALS Young Investigator Research Scholarship by the Deutsche Gesellschaft für Muskelkranke (DGM) and a Junior Research Grant by the Medical Faculty, University of Leipzig, to MO. JL was supported by a research fellowship from the Deutsche Forschungsgemeinschaft (DFG; award LA 3609/2-1). For the technical assistance, the authors thank Svetlana Tausch and Madlen Günther.

References

Alexianu, M.E., Ho, B.K., Mohamed, A.H., La Bella, V., Smith, R.G., Appel, S.H., 1994. The role of calcium-binding proteins in selective motoneuron vulnerability in amyotrophic lateral sclerosis. Ann. Neurol. 36, 846–858.

Bae, J.S., Simon, N.G., Menon, P., Vucic, S., Kiernan, M.C., 2013. The puzzling case of hyperexcitability in amyotrophic lateral sclerosis. J. Clin. Neurol. 9, 65–74.

Benyamin, B., Esko, T., Ried, J.S., Radhakrishnan, A., Vermeulen, S.H., Traglia, M., Gogele, M., Anderson, D., Broer, L., Podmore, C., Luan, J., Kutalik, Z., Sanna, S., van der Meer, P., Tanaka, T., Wang, F., Westra, H.J., Franke, L., Mihailov, E., Milani, L., Haldin, J., Winkelmann, J., Meitinger, T., Thiery, J., Peters, A., Waldenberger, M., Rendon, A., Jolley, J., Sambrook, J., Kiemeney, L.A., Sweep, F.C., Sala, C.F., Schwienbacher, C., Pichler, I., Hui, J., Demirkan, A., Isaacs, A., Amin, N., Steri, M., Waeber, G., Verweij, N., Powell, J.E., Nyholt, D.R., Heath, A.C., Madden, P.A., Visscher, P.M., Wright, M.J., Montgomery, G.W., Martin, N.G., Hernandez, D., Bandinelli, S., van der Harst, P., Uda, M., Vollenweider, P., Scott, R.A., Langenberg, C., Wareham, N.J., InterAct, C., van Duijn, C., Beilby, J., Pramstaller, P.P., Hicks, A.A., Ouwehand, W.H., Oexle, K., Gieger, C., Metspalu, A., Camaschella, C., Toniolo, D., Swinkels, D.W., Whitfield, J.B., 2014. Novel loci affecting iron homeostasis and their effects in individuals at risk for hemochromatosis. Nat. Commun. 5, 4926.

Carriedo, S.G., Sensi, S.L., Yin, H.Z., Weiss, J.H., 2000. AMPA exposures induce mitochondrial Ca(2+) overload and ROS generation in spinal motor neurons in vitro. J. Neurosci. 20, 240–250.

Carriedo, S.G., Yin, H.Z., Weiss, J.H., 1996. Motor neurons are selectively vulnerable to AMPA/kainate receptor-mediated injury in vitro. J. Neurosci. 16, 4069–4079.

Chang, Q., Martin, L.J., 2016. Voltage-gated calcium channels are abnormal in cultured spinal motoneurons in the G93A-SOD1 transgenic mouse model of ALS. Neurobiol. Dis. 93, 78–95.

Collings, M.A., Brewer, G.J., Evans, M.S., 1999. Calcium currents of embryonic and adult neurons in serum-free culture. Brain Res. Bull. 48, 73–78.

Cozzolino, M., Rossi, S., Mirra, A., Carri, M.T., 2015. Mitochondrial dynamism and the pathogenesis of amyotrophic lateral sclerosis. Front. Cell. Neurosci. 9, 31.

Feeney, C.J., Pennefather, P.S., Gyulkhandanyan, A.V., 2003. A cuvette-based fluorometric analysis of mitochondrial membrane potential measured in cultured astrocyte monolayers. J. Neurosci. Methods 125, 13–25.

Fuchs, A., Kutterer, S., Muhling, T., Duda, J., Schutz, B., Liss, B., Keller, B.U., Roeper, J., 2013. Selective mitochondrial Ca2+ uptake deficit in disease endstage vulnerable motoneurons of the SOD1G93A mouse model of amyotrophic lateral sclerosis. J. Physiol. 591 (Pt 10), 2723–2745.

Gavet, O., Pines, J., 2010. Progressive activation of CyclinB1-Cdk1 coordinates entry to mitosis. Dev Cell 18, 533–543.

Grosskreutz, J., Haastert, K., Dewil, M., Van Damme, P., Callewaert, G., Robberecht, W., Dengler, R., Van Den Bosch, L., 2007. Role of mitochondria in kainate-induced fast Ca2+ transients in cultured spinal motor neurons. Cell Calcium 42, 59–69.

Grosskreutz, J., Van Den Bosch, L., Keller, B.U., 2010. Calcium dysregulation in amyotrophic lateral sclerosis. Cell Calcium 47, 165–174.

Grynkiewicz, G., Poenie, M., Tsien, R.Y., 1985. A new generation of Ca2+ indicators with greatly improved fluorescence properties. J. Biol. Chem. 260, 3440–3450.

Gurney, M.E., Pu, H., Chiu, A.Y., Dal Canto, M.C., Polchow, C.Y., Alexander, D.D., Caliendo, J., Hentati, A., Kwon, Y.W., Deng, H.X., 1994. Motor neuron degeneration in mice that express a human Cu,Zn superoxide dismutase mutation. Science 264, 1772–1775.

Haastert, K., Grosskreutz, J., Jaeckel, M., Laderer, C., Bufler, J., Grothe, C., Claus, P., 2005. Rat embryonic motoneurons in long-term co-culture with Schwann cells–a system to investigate motoneuron diseases on a cellular level in vitro. J. Neurosci. Methods 142, 275–284.

Hajnoczky, G., Csordas, G., Das, S., Garcia-Perez, C., Saotome, M., Sinha Roy, S., Yi, M., 2006. Mitochondrial calcium signalling and cell death: approaches for assessing the role of mitochondrial Ca2+ uptake in apoptosis. Cell Calcium 40, 553–560.

Hu, J.H., Chernoff, K., Pelech, S., Krieger, C., 2003a. Protein kinase and protein phosphatase expression in the central nervous system of G93A mSOD overexpressing mice. J. Neurochem. 85, 422–431.

Hu, J.H., Zhang, H., Wagey, R., Krieger, C., Pelech, S.L., 2003b. Protein kinase and protein phosphatase expression in amyotrophic lateral sclerosis spinal cord. J. Neurochem. 85, 432–442.

Ingre, C., Roos, P.M., Piehl, F., Kamel, F., Fang, F., 2015. Risk factors for amyotrophic lateral sclerosis. Clin. Epidemiol. 7, 181–193.

Israelson, A., Arbel, N., Da Cruz, S., Ilieva, H., Yamanaka, K., Shoshan-Barmatz, V., Cleveland, D.W., 2010. Misfolded mutant SOD1 directly inhibits VDAC1 conductance in a mouse model of inherited ALS. Neuron 67, 575–587.

Jaenisch, N., Liebmann, L., Guenther, M., Hubner, C.A., Frahm, C., Witte, O.W., 2016. Reduced tonic inhibition after stroke promotes motor performance and epileptic seizures. Sci. Rep. 6, 26173.

Jahn, K., Grosskreutz, J., Haastert, K., Ziegler, E., Schlesinger, F., Grothe, C., Dengler, R., Bufler, J., 2006. Temporospatial coupling of networked synaptic activation of AMPA-type glutamate receptor channels and calcium transients in cultured motoneurons. Neuroscience 142, 1019–1029.

Jaiswal, M.K., 2014. Selective vulnerability of motoneuron and perturbed mitochondrial calcium homeostasis in amyotrophic lateral sclerosis: implications for motoneurons specific calcium dysregulation. Mol. Cell Ther. 2, 26.

Jaiswal, M.K., Zech, W.D., Goos, M., Leutbecher, C., Ferri, A., Zippelius, A., Carri, M.T., Nau, R., Keller, B.U., 2009. Impairment of mitochondrial calcium handling in a mtSOD1 cell culture model of motoneuron disease. BMC Neurosci. 10, 64.

Joiner, M.L., Koval, O.M., Li, J., He, B.J., Allamargot, C., Gao, Z., Luczak, E.D., Hall, D.D., Fink, B.D., Chen, B., Yang, J., Moore, S.A., Scholz, T.D., Strack, S., Mohler, P.J., Sivitz, W.I., Song, L.S., Anderson, M.E., 2012. CaMKII determines mitochondrial stress responses in heart. Nature 491, 269–273.

Joshi, D.C., Singh, M., Krishnamurthy, K., Joshi, P.G., Joshi, N.B., 2011. AMPA induced Ca2+ influx in motor neurons occurs through voltage gated Ca2+ channel and Ca2+ permeable AMPA receptor. Neurochem. Int. 59, 913–921.

Joshi, D.C., Tewari, B.P., Singh, M., Joshi, P.G., Joshi, N.B., 2015. AMPA receptor activation causes preferential mitochondrial Ca(2)(+) load and oxidative stress in motor neurons. Brain Res. 1616, 1–9.

Kiernan, M.C., Vucic, S., Cheah, B.C., Turner, M.R., Eisen, A., Hardiman, O., Burrell, J.R., Zoing, M.C., 2011. Amyotrophic lateral sclerosis. Lancet 377, 942–955.

King, A.E., Woodhouse, A., Kirkcaldie, M.T., Vickers, J.C., 2016. Excitotoxicity in ALS: Overstimulation, or overreaction? Exp. Neurol. 275 (Pt 1), 162–171.

Kirichok, Y., Krapivinsky, G., Clapham, D.E., 2004. The mitochondrial calcium uniporter is a highly selective ion channel. Nature 427, 360–364.

Krieger, C., Lanius, R.A., Pelech, S.L., Shaw, C.A., 1996. Amyotrophic lateral sclerosis: the involvement of intracellular Ca2+ and protein kinase C. Trends Pharmacol. Sci. 17, 114–120.

Ladewig, T., Kloppenburg, P., Lalley, P.M., Zipfel, W.R., Webb, W.W., Keller, B.U., 2003. Spatial profiles of store-dependent calcium release in motoneurones of the nucleus hypoglossus from newborn mouse. J. Physiol. 547 (Pt 3), 775–787.

Lautenschlager, J., Prell, T., Ruhmer, J., Weidemann, L., Witte, O.W., Grosskreutz, J., 2013. Overexpression of human mutated G93A SOD1 changes dynamics of the ER mitochondria calcium cycle specifically in mouse embryonic motor neurons. Exp. Neurol. 247, 91–100.

Lips, M.B., Keller, B.U., 1999. Activity-related calcium dynamics in motoneurons of the nucleus hypoglossus from mouse. J. Neurophysiol. 82, 2936–2946.

Marchi, S., Pinton, P., 2014. The mitochondrial calcium uniporter complex: molecular components, structure and physiopathological implications. J. Physiol. 592, 829–839.

Martin, L.J., 2011. Mitochondrial pathobiology in ALS. J. Bioenerg. Biomembr. 43, 569–579.

Martin, L.J., Gertz, B., Pan, Y., Price, A.C., Molkentin, J.D., Chang, Q., 2009. The mitochondrial permeability transition pore in motor neurons: involvement in the pathobiology of ALS mice. Exp. Neurol. 218, 333–346.

Muhling, T., Duda, J., Weishaupt, J.H., Ludolph, A.C., Liss, B., 2014. Elevated mRNA-levels of distinct mitochondrial and plasma membrane Ca(2+) transporters in individual hypoglossal motor neurons of endstage SOD1 transgenic mice. Front. Cell Neurosci. 8, 353.

Palecek, J., Lips, M.B., Keller, B.U., 1999. Calcium dynamics and buffering in motoneurones of the mouse spinal cord. J. Physiol. 520 Pt 2, 485–502.

Pfaffl, M.W., 2001. A new mathematical model for relative quantification in real-time RT-PCR. Nucleic Acids Res. 29, e45.

Prell, T., Lautenschlager, J., Witte, O.W., Carri, M.T., Grosskreutz, J., 2012. The unfolded protein response in models of human mutant G93A amyotrophic lateral sclerosis. Eur. J. Neurosci. 35, 652–660.

Qiu, J., Tan, Y.W., Hagenston, A.M., Martel, M.A., Kneisel, N., Skehel, P.A., Wyllie, D.J., Bading, H., Hardingham, G.E., 2013. Mitochondrial calcium uniporter Mcu controls excitotoxicity and is transcriptionally repressed by neuroprotective nuclear calcium signals. Nat. Commun. 4, 2034.

Rapizzi, E., Pinton, P., Szabadkai, G., Wieckowski, M.R., Vandecasteele, G., Baird, G., Tuft, R.A., Fogarty, K.E., Rizzuto, R., 2002. Recombinant expression of the voltage-dependent anion channel enhances the transfer of Ca2+ microdomains to mitochondria. J. Cell Biol. 159, 613–624.

Rosen, D.R., Siddique, T., Patterson, D., Figlewicz, D.A., Sapp, P., Hentati, A., Donaldson, D., Goto, J., O'Regan, J.P., Deng, H.X., Rahmani, Z., Krizus, A., McKenna-Yasek, D., Cayabyab, A., Gaston, S.M., Berger, R., Tanzi, R.E., Halperin, J.J., Herzfeldt, B., Van den Bergh, R., Hung, W., Bird, T., Deng, G., Mulder, D.W., Smyth, C., Laing, N.G., Soriano, E., Pericak–Vance, M.A., Haines, J., Rouleau, G.A., Gusella, J.S., Horvitz, H.R., Brown Jr, R.H., 1993. Mutations in Cu/Zn superoxide dismutase gene are associated with familial amyotrophic lateral sclerosis. Nature 362, 59–62.

Stout, A.K., Raphael, H.M., Kanterewicz, B.I., Klann, E., Reynolds, I.J., 1998. Glutamate-induced neuron death requires mitochondrial calcium uptake. Nat. Neurosci. 1, 366–373.

Tadic, V., Prell, T., Lautenschlaeger, J., Grosskreutz, J., 2014. The ER mitochondria calcium cycle and ER stress response as therapeutic targets in amyotrophic lateral sclerosis. Front. Cell Neurosci. 8, 147.

Van Den Bosch, L., Van Damme, P., Bogaert, E., Robberecht, W., 2006. The role of excitotoxicity in the pathogenesis of amyotrophic lateral sclerosis. Biochim. Biophys. Acta 1762, 1068–1082.

Van den Bosch, L., Van Damme, P., Vleminckx, V., Van Houtte, E., Lemmens, G., Missiaen, L., Callewaert, G., Robberecht, W., 2002. An alpha-mercaptoacrylic acid derivative (PD150606) inhibits selective motor neuron death via inhibition of kainate-induced Ca2+ influx and not via calpain inhibition. Neuropharmacology 42, 706–713.

Van Den Bosch, L., Vandenberghe, W., Klaassen, H., Van Houtte, E., Robberecht, W., 2000. Ca(2+)-permeable AMPA receptors and selective vulnerability of motor neurons. J. Neurol. Sci. 180, 29–34.

Williams, G.S., Boyman, L., Chikando, A.C., Khairallah, R.J., Lederer, W.J., 2013. Mitochondrial calcium uptake. Proc. Natl. Acad. Sci. U. S. A. 110, 10479–10486.

Wyatt, C.N., Buckler, K.J., 2004. The effect of mitochondrial inhibitors on membrane currents in isolated neonatal rat carotid body type I cells. J. Physiol. 556 (Pt 1), 175–191.